Geoscience Letters

RESEARCH LETTER

Open Access

The upper-level atmospheric pathway of ENSO's impact on winter rainfall in southern China

Jiawen Zhang[1,4], Kaiming Hu[1,3*], Gang Huang[1,2,4*] and Ya Wang[1]

Abstract

Using observational and reanalysis datasets from 1979 to 2023, this study investigates the role of upper- and middle-tropospheric circulation anomalies in mediating the influence of El Niño-Southern Oscillation (ENSO) on South China winter precipitation (SCWP). The results show that El Niño events trigger a prominent quasi-barotropic cyclonic anomaly over East Asia, with peak intensity occurring between 150 and 200-hPa in the upper troposphere. Eastward of this anomaly, mid-tropospheric southerly wind anomalies induce warm air advection along the East Asian coastline, which enhances vertical upward motion. Additionally, the differential vertical vorticity advection—driven by stronger vorticity anomalies and amplified zonal winds in the upper troposphere compared to the lower levels—further intensifies the ascending motion along the eastern flank of the cyclonic anomaly. Consequently, this upper- and middle-tropospheric anomalous cyclone creates a corridor of ascending motion that extends from southern China to the region south of Japan, leading to the development of positive precipitation anomalies in the region. This finding could help improve the seasonal forecast skill of SCWP.

Keywords ENSO, Winter precipitation in southern China, Upper layer

Introduction

In winter, East Asia is dominated by cold and dry winter monsoon (Ding 1990; Huang et al. 2004; Wang and Lu 2013). As a result, wintertime rainfall is less than the other seasons in most regions, but it is still large and shows a strong year-to-year variability in southern China (Zhou and Wu 2010; Wang and Feng 2011; Li and Ma 2012). Given the large population in southern China, precipitation anomalies can lead to substantial economic and social impacts (Wang and Feng 2011). For example, a severe winter flooding event hit south China in the winter of 2015/16 (Guo et al. 2019; Li et al. 2020), resulting in severe impacts on agriculture and transport. Previous studies show that the interannual variability of precipitation in southern China is likely affected by a series of factors, including El Niño-Southern Oscillation (ENSO) (Zhang et al. 1996; Wu et al. 2003; Li and Ma 2012), sea surface temperature (SST) anomalies in the South China Sea (Zhou 2010) and the Atlantic (Liu et al. 2012, 2020), the Pacific Decadal Oscillation (Chen et al. 2013), and the East Asian winter monsoon (Wang and Chen 2010; Zhou and Wu 2010). Among these factors, ENSO's relatively long persistence makes it a primary driver of the seasonal

*Correspondence:
Kaiming Hu
hkm@mail.iap.ac.cn
Gang Huang
hg@mail.iap.ac.cn
[1] Key Laboratory of Earth System Numerical Modeling and Application, Institute of Atmospheric Physics, Chinese Academy of Sciences, Beijing, China
[2] Laboratory for Regional Oceanography and Numerical Modeling, Qingdao National Laboratory for Marine Science and Technology, Qingdao, China
[3] China Collaborative Innovation Center on Forecast and Evaluation of Meteorological Disasters (CIC-FEMD), Nanjing University of Information Science & Technology, Nanjing, China
[4] College of Earth and Planetary Sciences, University of Chinese Academy of Sciences, Beijing, China

predictability of southern China winter precipitation (SCWP). The skillful seasonal prediction of SCWP in climate models depends mostly on the successful representation of the observed ENSO teleconnection (Lu et al. 2017). Therefore, understanding how ENSO affects winter rainfall in southern China is crucial.

One pathway through which ENSO impacts SCWP is by inducing changes in low-level circulation over the Northwest Pacific. During El Niño winters, a low-level anticyclonic atmospheric circulation anomaly develop over the Northwest Pacific (Wang et al. 2000). This anomaly is driven by local ocean surface cooling and remotely forced subsidence associated with warming in the central and eastern Pacific warming (Zhang et al. 1996; Wang et al. 2000; Li et al. 2017; Wu et al. 2017). On the northwest flank of the anticyclonic anomaly, southwesterly wind anomalies enhance the transport of water vapor from the tropical ocean to southern China, resulting in increased winter rainfall in the region (Wu et al. 2003).

In addition to generating low-level circulation anomaly over the Northwest Pacific, ENSO also significantly influences upper- and middle-tropospheric circulation patterns across East Asia. There are three equatorial symmetric Rossby wave dumbbells of alternating signs during El Niño mature phase (Adames and Wallace 2017). As part of these Rossby wave dumbbells, cyclonic and anticyclonic anomalies are observed in the upper troposphere over East Asia during El Niño and La Niña events, respectively. Previous studies reported that ENSO can impact on SCWP by exciting subtropical jet-trapped Rossby waves and altering the jet's latitudinal position (Liu et al. 2012; Li and Sun 2015; Hu et al. 2018; Gao et al. 2020; Li et al. 2020). However, the El Niño-associated upper-layer anomalous cyclone over East Asia cannot be attributed to jet-trapped Rossby waves, as it exhibits a symmetric counterpart in the Southern Hemisphere. The impact of the El Niño-associated upper-level anomalous cyclone over East Asia on SCWP remains poorly understood.

In this study, we aim to address the key issues. We found the El Niño-associated upper-level anomalous cyclone over East Asia plays an important role in ENSO's impact on SCWP. For simplicity, we refer to the processes as the upper-layer pathway related to most discussed low-level pathway. The remainder of the paper is organized as follows. Section "Data and methods" describes the data used in the analysis. Section "The upper-level pathways of ENSO impact on SCWP" examines the dynamic processes through which upper-tropospheric circulation influences ENSO-related SCWP anomalies. Finally, Section "Summary" provides a summary of the findings.

Data and methods

The monthly mean atmospheric circulation and temperature fields are from the fifth-generation ECMWF reanalysis for the global climate and weather (ERA5; (Hersbach et al. 2020) at a resolution of 2.5° latitude × 2.5° longitude from 1979 to the 2023. Monthly global precipitation gridded at 2.5° × 2.5° horizontal resolution is from the Global Precipitation Climatology Project (GPCP) dataset (Adler et al. 2003). Monthly global gridded SST dataset is from the U.K. Met Office Hadley Centre (HadISST), with a resolution of 1° × 1° (Rayner et al. 2003). The interannual variability of ENSO is quantified using the December–February [D(0)JF(1)] mean Niño3.4 index, calculated from SST anomalies averaged over the region 5°S–5°N, 170°W–120°W. The statistical significance of the results was assessed using a two-tailed Student's t-test.

The observed results are validated using AMIP (Atmospheric Model Intercomparison Project) simulations from eleven Coupled Model Intercomparison Project Phase 6 (CMIP6) models, including BCC-CSM2-MR, CESM2, CNRM-CM6-1, CanESM5, E3SM-1–0, GFDL-CM4, HadGEM3-GC31-LL, IPSL-CM6A-LR, MIROC6, MRI-ESM2-0, and TaiESM1. The eleven models were selected based on their availability of all required variables for our analyses. These simulations are forced by observed sea surface temperatures (SSTs) during the period 1979–2014. For simplicity, we compute the ensemble mean of the 11 models' simulations and base our analysis on this aggregated result. More detailed online model documentations for the CMIP6 models are available at https://pcmdi.llnl.gov/CMIP6/.

The upper-level pathways of ENSO impact on SCWP

Figure 1a–c shows the D(0)JF(1) circulation anomalies at 150, 500 and 850-hPa, respectively, regressed onto the simultaneous normalized Niño3.4 index over the period from 1979 to 2023. Notably, pronounced cyclonic anomalies are observed over East Asia at both 150 hPa and 500 hPa, with the anomalies at 150 hPa exhibiting a greater magnitude compared to those at 500 hPa. The maximum anomaly occurred between 150 and 200 hPa in the upper troposphere (Supplementary Fig. 1). In the tropical Indo-Western Pacific regions, an anomalous anticyclone is evident at 850-hPa. To the north of this low-level anticyclone and east of the upper-level cyclonic anomaly, a band of positive rainfall extends from South China to the south of Japan (Fig. 1c). The AMIP simulations (Fig. 1d–f) capture the ENSO-related circulation patterns, vertical velocity, and precipitation anomalies with remarkable consistency compared to observations, suggesting these anomalies are primarily driven by ENSO-related SST forcing. While previous research (Wu et al. 2003, 2010; Ke et al. 2019; Zhang et al. 2021; Huang

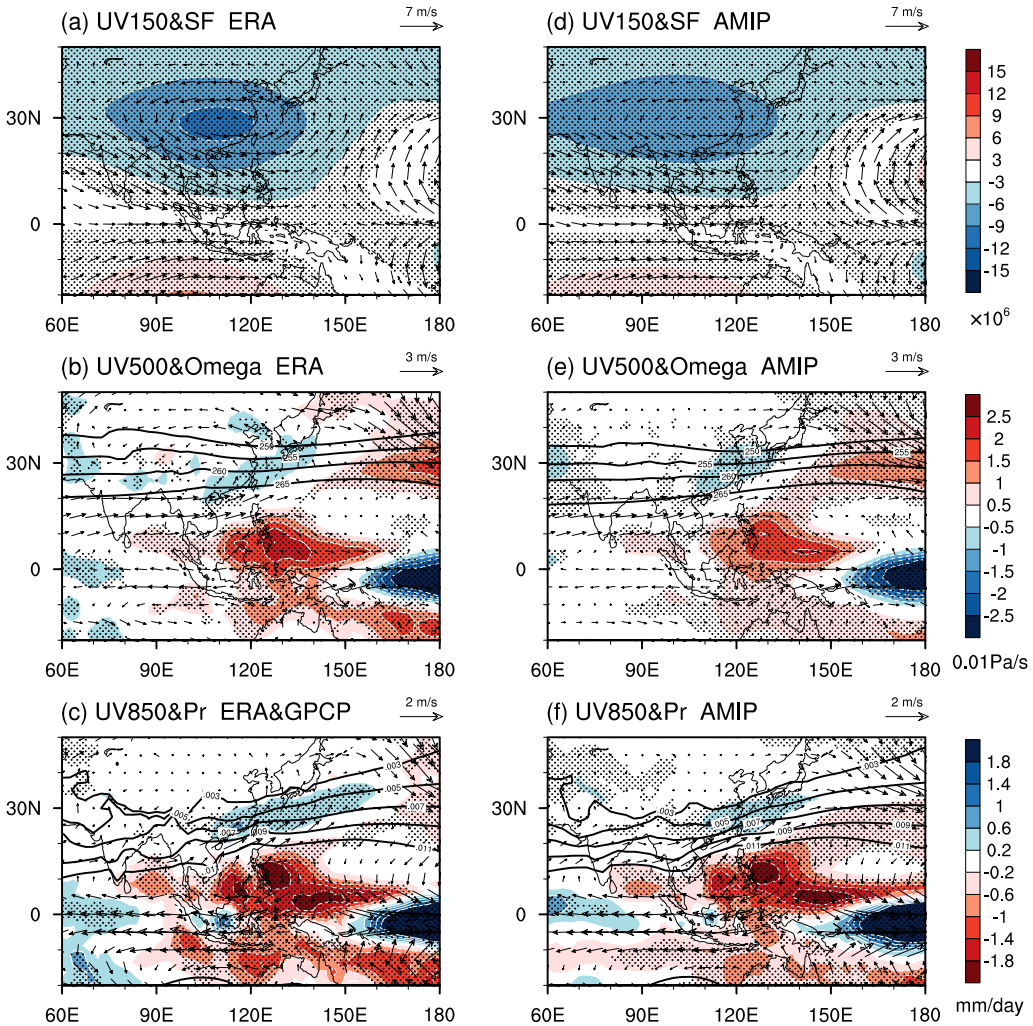

Fig. 1 D(0)JF(1) circulation anomalies associated with ENSO. **a** Regression of observed D(0)JF(1)wind (vectors) and stream function (shaded) at 150 hPa onto the normalized D(0)JF(1) Niño3.4 index from 1979 to 2023; **b** regression of observed wind (vectors) and omega (shaded) at 500 hPa onto the Niño3.4 index, with contours denoting the D(0)JF(1) mean 500-hPa temperature (unit:k); **c** regression of observed 850-hPa wind (vectors) and precipitation (shaded) onto the Niño3.4 index, with contours representing the D(0)JF(1) mean lower-level specific humidity (vertical average from the surface to 850 hPa, unit: kg/kg). The right **d**–**f** shows the same as the left panel but for ensemble mean of 11 AMIP simulations from 1979 to 2014. Dots indicate regions where anomalies pass the 95% confidence level test based on statistical significance

et al. 2023) have attributed this rainfall belt primarily to enhanced vapor transport facilitated by the low-level anticyclone, our analysis reveals that the rainfall belt also coincides with significant upward motion anomalies at 500 hPa, extending from South China to the region south of Japan (Fig. 1b). This suggests that dynamic processes associated with vertical motion may play a pivotal role in the formation of the anomalous rainfall belt.

In order to analyze the mechanisms of vertical motion, a diagnosis employing the linearized omega equation has been performed followed (Kosaka and Nakamura 2010):

$$\begin{aligned}\omega' = &\underbrace{\left(\nabla^2+\frac{f^2}{\sigma^2}\frac{\partial^2}{\partial P^2}\right)^{-1}\frac{f}{\sigma}\frac{\partial}{\partial P}\left[\overline{\mathbf{V}}\cdot\nabla\zeta'+\mathbf{V}'\cdot\nabla(f+\overline{\zeta})\right]}_{\omega_{vor}}\\ &+\underbrace{\left(\nabla^2+\frac{f^2}{\sigma^2}\frac{\partial^2}{\partial P^2}\right)^{-1}\frac{R}{\sigma P}\nabla^2\left(\overline{\mathbf{V}}\cdot\nabla T'+\mathbf{V}'\cdot\nabla\overline{T}\right)}_{\omega_T}\\ &+\underbrace{\left[-\left(\nabla^2+\frac{f^2}{\sigma^2}\frac{\partial^2}{\partial P^2}\right)^{-1}\frac{R}{\sigma P c_p}\nabla^2 Q\right]}_{\omega_Q}\end{aligned} \tag{1}$$

where the overbar and prime symbols denote climatological mean quantities for D(0)JF(1) and the regressed anomalies, respectively. The static stability, σ, is defined as $\sigma = (R/P)\left(R\overline{T}/C_pP - d\overline{T}/dP\right)$, with ζ representing

relative vorticity, f the Coriolis parameter, R the gas constant, T air temperature, **V** horizontal wind, and Q diabatic heating. We perform the Laplacian inversion utilizing functions from the Math Kernel Library. The vertical derivative at the boundary is designated as a missing value, thereby constraining the program to solve for omega exclusively within the inner layer. The first term in the right–hand-side of Eq. (1) signifies the contribution arising from the vertical difference of vorticity advection. The second term represents the influence of horizontal temperature advection, while the third term represents the effect of diabatic heating. The detailed physical mean of each term can refer to Hoskins et al. (2003). For brevity, we employ the abbreviations, ω_{vor}, ω_T, and ω_Q to denote these three terms, respectively.

Figure 2a–d presents the spatial distribution of ω_{vor}, ω_T, ω_Q, and their combined total, respectively, while Fig. 2e displays the observed 500-hPa vertical velocity anomalies regressed onto the normalized D(0)JF(1) Nino3.4 index. The combined total (Fig. 2d) demonstrates strong consistency with the observed vertical velocity anomalies (Fig. 2e) in both magnitude and spatial pattern, indicating that the omega anomalies are primarily driven by the contributions of these three components. The ω_{vor} exhibits negative values centered over the eastern part of anomalous cyclone in East Asia. As shown in Fig. 1, the cyclonic anomaly over East Asia are most pronounced in the upper troposphere. Combined with the fact that the climatological zonal wind is also strongest in the upper troposphere, the positive vorticity advection east of the East Asian cyclone is more intense in the upper troposphere compared to the lower troposphere. According to the omega equation, this vertical difference in vorticity advection induces ascending motion, explaining the negative ω_{vor} over eastern China. The ω_T shows negative values centered over southern China and Korean peninsula. Since ω_T results from horizontal temperature advection, the ascending motion, induced by these negative values, is likely driven by warm air advection associated with anomalous mid-tropospheric southerly anomalies on the east frank of East Asian anomalous cyclone (Fig. 1b). The ω_Q displays negative values from southern China to the sea south of Japan, which arise from diabatic heating due to anomalous precipitation.

All three components exhibit negative values over southern China, suggesting that each contributes to

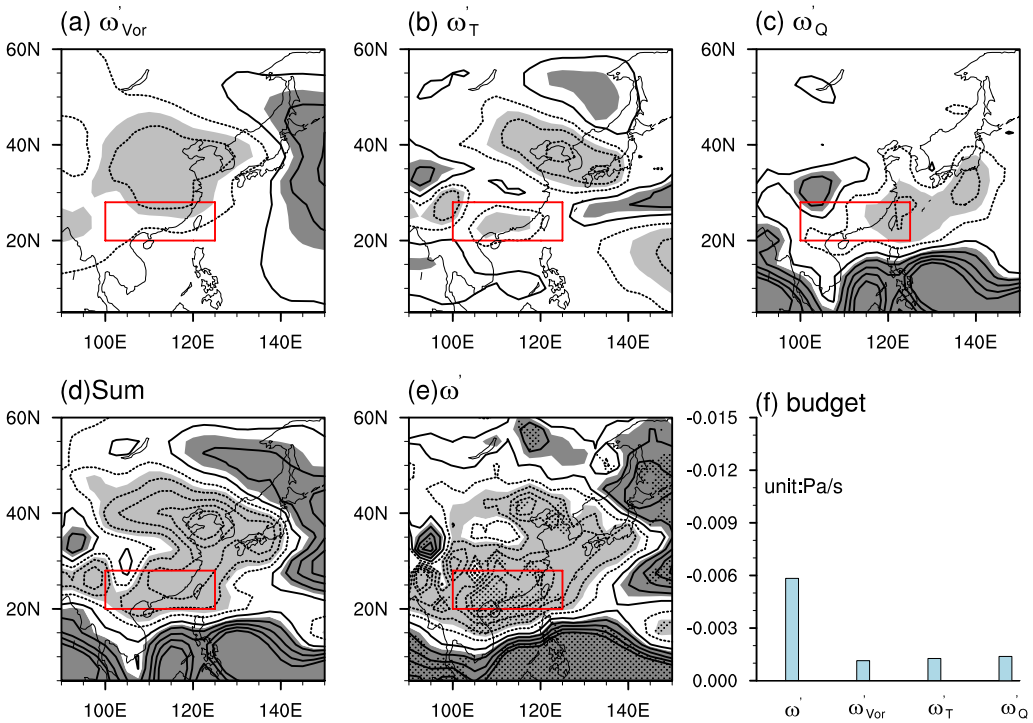

Fig. 2 ENSO-related omega anomalies and their components at 500 hPa. **a** Spatial distribution of ω_{vor} (vorticity advection contribution); **b** ω_T (temperature advection contribution); **c** ω_Q (diabatic heating contribution); **d** their combined total, calculated by Eq. (1). **e** Observed 500-hPa vertical velocity anomalies regressed onto the normalized D(0)JF(1) Niño3.4 index during 1979–2023. **f** Area-averaged values of the three terms (ω_{vor}, ω_T, ω_Q) and the ERA5 vertical velocity anomaly over southern China, delineated by the red box spanning 100°E–125°E and 20°N–28°N. The contour interval in a–e is $0.2(\pm 0.1, \pm 0.3, \pm 0.5, \cdots) \times 10^{-2} Pa/s$, with light gray shading indicating values below $-0.2 \times 10^{-2} Pa/s$ and dark gray above $0.2 \times 10^{-2} Pa/s$. Dots in e denote regressions that pass the 95% confidence level

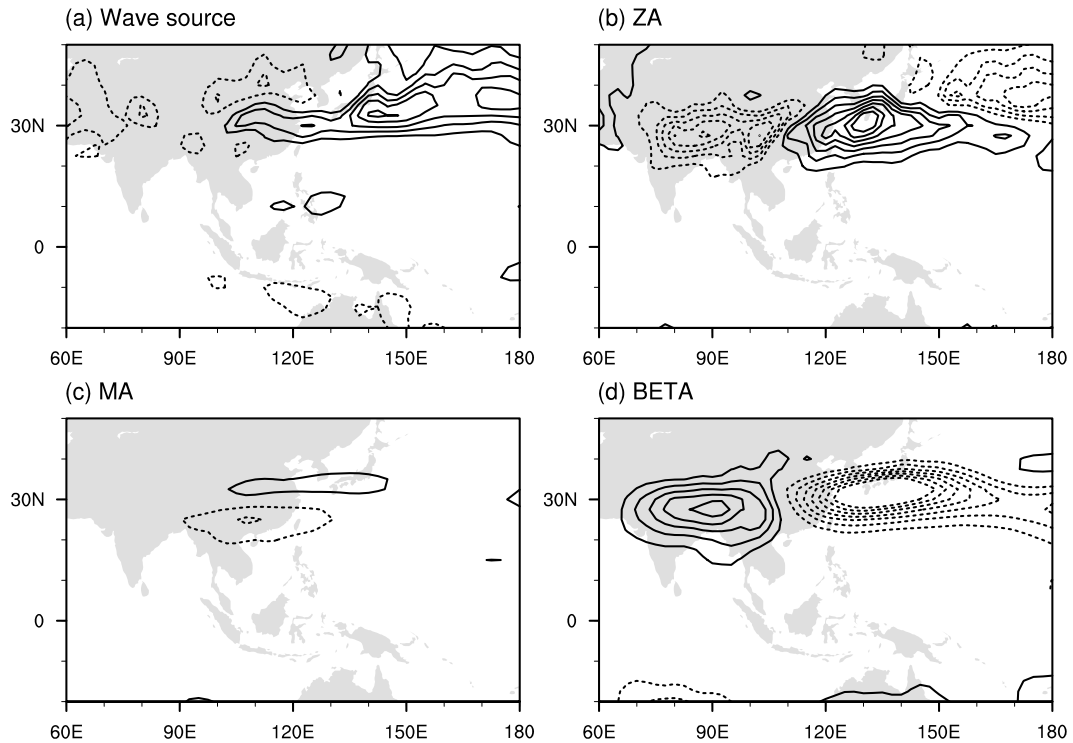

Fig. 3 Vorticity budget at 150-hPa. **a** Rossby wave source; **b** zonal advection term; **c** meridional advection term; **d** β term for 150-hPa D(0)JF(1) vorticity anomalies regressed onto the normalized D(0)JF(1) Niño3.4 index during 1979–2023, based on Eq. (2). Solid (dashed) contours denote positive (negative) values, with a contour interval 4 ($\pm 2, \pm 4, \pm 8, \pm 10, \cdots$) $\times\ 10^{-11} s^{-2}$

the ascending motion anomalies in this region. Figure 2f further quantifies the area-averaged values of the three terms and vertical velocity anomaly in southern China, delineated by the red box spanning 100–125°E and 20–28°N. The area-averaged contributions of ω_{vor}, ω_T, and ω_Q account for 20%, 22%, and 24% of the vertical velocity anomalies, respectively. The term ω_Q should be considered a feedback term, as ascending motion induced diabatic heating, which in turn enhances ascending motion. In contrast, the 500 hPa ω_{vor} and ω_T are directly related to the ENSO-induced upper layer anomalous cyclone over East Asia. Thus, ENSO can influence vertical motion over southern China by modulating the upper-level circulation, which subsequently impacts vorticity advection and temperature advection in the region. The contributions from both vorticity advection differences and thermal advection are also evident in the AMIP simulations (Supplementary Fig. 2).

It is noteworthy that there are some differences between the spatial patterns of 500-hPa vertical motion anomalies (Fig. 2e) and precipitation anomalies (Fig. 1c). For instance, significant ascending motion anomalies are observed over the Korean Peninsula, but the corresponding precipitation anomalies are not significant in this region. This discrepancy can likely be attributed to insufficient moisture availability, even in the presence of ascending motion. As shown in Fig. 1c, f, a strong meridional gradient of specific humidity is evident over East Asia, with a contour of 0.011 kg/kg around 20°N and a contour of 0.003 kg/kg around 32°N. In relatively dry regions (specific humidity below 0.003 kg/kg), significant ascending motion does not correspond to significant positive precipitation anomalies. Therefore, ascending motion alone is not sufficient to generate precipitation if the atmospheric column lacks adequate water vapor. This highlights the critical role of moisture supply in determining precipitation patterns. From this perspective, both enhanced vapor transport driven by low-level circulation and ascending motion induced by upper-level circulation are essential for the formation and maintenance of the SCWP anomalies in ENSO years.

Moreover, to analyze how ENSO induces upper-level circulation anomalies over East Asia, we conduct an analysis of the vorticity budget based on the linearized vorticity equation (Kosaka and Nakamura 2006):

$$S \underbrace{-\overline{u}_{\psi}\frac{\partial \zeta'}{\partial x}}_{ZA} \underbrace{-\overline{v}_{\psi}\frac{\partial \zeta'}{\partial y}}_{MA} \underbrace{-u'_{\psi}\frac{\partial \overline{\zeta}}{\partial x} - v'_{\psi}\frac{\partial (f+\overline{\zeta})}{\partial y}}_{\beta} - (residuals) = 0 \quad (2)$$

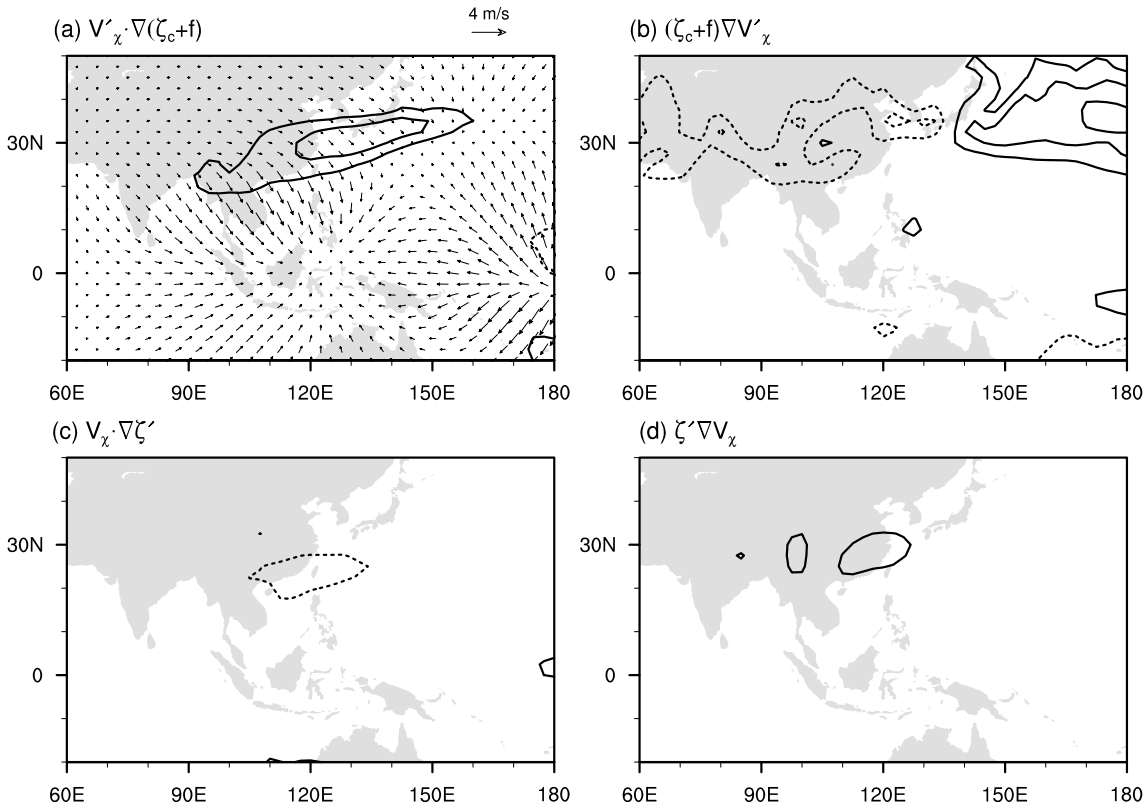

Fig. 4 Components of the 150-hPa wave source shown in Fig. 3a. **a** Advection of mean vorticity by the perturbation divergent wind; **b** vortex stretching induced by the perturbation divergent wind; **c** advection of perturbation vorticity by the mean divergent wind; and **d** vortex stretching caused by the mean divergent wind, calculated based on Eq. (3). Vectors in a represent the divergent wind components regressed onto the normalized D(0)JF(1) Niño3.4 index during 1979–2023. Solid (dashed) contours denote positive (negative) values, with a contour interval 4 $(\pm 2, \pm 4, \pm 8, \pm 10, \cdots) \times 10^{-11} s^{-2}$

where S represents the linearized barotropic Rossby wave source (Sardeshmukh and Hoskins 1988):

$$S = -\mathbf{u}'_\chi \cdot \nabla_H\left(f + \overline{\zeta}\right) - \left(f + \overline{\zeta}\right)\nabla_H \cdot \mathbf{u}'_\chi - \overline{\mathbf{u}}_\chi \cdot \nabla_H \zeta' - \zeta' \nabla_H \cdot \overline{\mathbf{u}}_\chi. \quad (3)$$

In Eqs. (2) and (3),$\mathbf{u}_\psi = (u_\psi, v_\psi)$ and $\mathbf{u}_\chi = (u_\chi, v_\chi)$ represent the rotational and divergent wind components, respectively, while ζ denotes relative velocity. The overbars and primes denote the D(0)JF(1) climatological mean and the monthly anomalies regressed onto the normalized D(0)JF(1) Nino3.4 index, respectively. The terms *ZA* and *MA* correspond to the advections of anomalous vorticity by the climatological zonal and meridional winds, respectively, and the β term represents the horizontal advection of the mean absolute vorticity by anomalous winds. Vertical advection, tilting and nonlinear effects are incorporated into the residual terms. A positive value of any given term indicates a tendency toward increasing cyclonic vorticity.

Figure 3a–d illustrates the relative contributions of each dynamical term to the 150-hPa vorticity anomalies. A pronounced positive wave source is evident around 30°N latitude, extending from East Asia to the North Pacific (Fig. 3a). Notably, the anomalous cyclone over East Asia corresponds to a positive wave source (Fig. 1a), demonstrating a robust dynamical linkage between wave source and the anomalous cyclone. The ZA term exhibits a dipole structure, with negative values to the west of the East Asian cyclone and positive values to its east. In contrast, the β term displays a comparable magnitude but an opposing spatial pattern. This anti-phase relationship suggests that the advection of perturbation vorticity by mean flow is largely counterbalanced by the β effect. The value of MA (Fig. 3c) is negative in South China, and its magnitude is comparable to the positive value of the

wave source (Fig. 3a). Thus, the Rossby wave source term in the South China region is primarily balanced by MA. The values of residuals, which are small in magnitude and spatially scattered (not shown), suggest a negligible contribution. This dynamical balance implies that the upper layer East Asian cyclone represents a stationary wave response to an ENSO-induced Rossby wave source.

The wave source term, as described in Eq. (3), can be linearly decomposed into four distinct components (Sardeshmukh and Hoskins 1988): (1) the advection of mean vorticity by the perturbation divergent wind; (2) vortex stretching induced by the perturbation divergent wind; (3) the advection of perturbation vorticity by the mean divergent wind; and (4) vortex stretching caused by the mean divergent wind. Figure 4a–d shows the four components of wave source term, respectively. During periods of a positive D(0)JF(1) Nino3.4 index, convergence wind anomalies are observed in the western Pacific (Fig. 4a). The southward divergent wind over East Asia and the Northwest Pacific contributes to positive mean vorticity advection near East Asian Jet (Fig. 4a), a region marked by a strong meridional vorticity gradient. The vortex stretching term induced by the mean divergent wind (Fig. 4d) is also positive over eastern China, with a magnitude approximately half that of the vorticity advection by perturbation divergent winds. The results suggest that the advection of mean vorticity by El Niño-induced perturbation divergent winds serves as the primary mechanism generating the East Asian anomalous cyclone, while vortex stretching associated with climatological convergence winds provides secondary intensification. These findings are consistent with Kuramochi and Ueda (2023), who demonstrated that both anomalous vorticity advection and background vortex stretching contribute to shaping East Asian circulation patterns. In contrast, the remaining two components, (1) the advection of perturbation vorticity by the mean divergent wind (Fig. 4b); and (2) the nonlinear advection of perturbation vorticity by perturbation divergent winds (Fig. 4c), both exhibit negative values over East Asia. These terms consequently act to dampen the upper-tropospheric anomalous cyclone in this region. The results demonstrate that the upper-tropospheric anomalous cyclone over East Asia primarily arises from two key dynamical processes: (1) the advection of mean vorticity by perturbation divergent winds; and (2) vortex stretching induced by the mean divergent wind, consistent with previous studies (Sardeshmukh and Hoskins 1988; Kuramochi and Ueda 2023).

Summary

In this study, we investigate the influence of ENSO on the SCWP using reanalysis data spanning from 1970 to 2023. Our findings reveal that ENSO exerts its impact through a dynamic upper-level pathway. Specifically, El Niño-induced changes in the Walker circulation enhance upper-level convergence over the tropical western Pacific, triggering a southward divergent flow. This flow facilitates positive vorticity advection, leading to the formation of an anomalous cyclone over East Asia in both the upper and middle troposphere. The climatological convergence winds to the east of Tibet Plateau further intensify the anomalous cyclone by vortex stretching effect. The resulting quasi-barotropic cyclone drives upward motion at 500 hPa over southern China, primarily through modifications in vorticity and temperature advection. The increased ascent, coupled with amplified low-level moisture transport, generates significant positive precipitation anomalies. Our results underscore the pivotal role of both upper-level dynamics and low-level moisture flux in the modulation of SCWP during ENSO phases.

In addition to this upper-level pathway, ENSO influences the SCWP by exciting subtropical jet-trapped Rossby waves (Hu et al. 2018) and altering the jet's latitudinal positions (Gao et al. 2020). Furthermore, interannual variability in the Australian summer monsoon can independently influence East Asian upper-level circulation by exciting cross-equatorial divergent winds that propagate toward East Asia (Sekizawa et al. 2021). These multiple interacting processes increase the complexity of ENSO's impact on SCWP. A comprehensive investigation of their synergistic effects could potentially improve SCWP forecast skill.

Abbreviations

ENSO	El Niño-Southern Oscillation
SCWP	South China winter precipitation
SST	Sea surface temperature

Supplementary Information

The online version contains supplementary material available at https://doi.org/10.1186/s40562-025-00398-2.

Additional file 1: Supplementary Fig. S1. Regression of D(0)JF(1) zonal mean (90–120°E) geopotential height (m) onto the normalized D(0)JF(1) Niño3.4 index during 1979–2023. Dots indicate regressions that are statistically significant at the 95% confidence level. Supplementary Fig. 2. ENSO-related omega anomalies and their components at 500 hPa in AMIP simulations. **a** Spatial distribution of ω_{vor} (vorticity advection contribution); **b** ω_T (temperature advection contribution); **c** 500-hPa vertical velocity anomalies regressed onto the normalized D(0)JF(1) Niño3.4 index during 1979–2014. The contour interval in **a**–**c** is $0.2(\pm 0.1, \pm 0.3, \pm 0.5, \cdots) \times 10^{-2} Pas^{-1}$, with light gray shading indicating values below $-0.2 \times 10^{-2} Pas^{-1}$ and dark gray above $0.2 \times 10^{-2} Pas^{-1}$. Dots in **c** denote regressions that pass the 95% confidence level.

Acknowledgements

Not applicable.

Author contributions

JZ and KH conceived the research idea, performed data analysis, generated figures and drafted the manuscript. KH and GH supervised the research, coordinated the project and serve as the corresponding author responsible

for communication and final manuscript approval. YW critically revised and polished the manuscript for clarity, logical coherence, and language refinement. All authors reviewed and approved the final version of the manuscript.

Funding
This work is supported by the National Natural Science Foundation of China (Grants 42175040 and 42475046) and the Youth Innovation Promotion Association of CAS (2021072).

Data availability
The HadISST dataset (Rayner et al. 2003) is available at https://www.metoffice.gov.uk/hadobs/hadisst/. The ERA5 dataset (Hersbach et al. 2020) can be obtained at https://www.ecmwf.int/en/forecasts/dataset/ecmwf-reanalysis-v5. The monthly GPCP dataset (Adler et al. 2003) is available at https://climatedataguide.ucar.edu/climate-data/gpcp-monthly-global-precipitation-climatology-project. The AMIP data is from https://pcmdi.llnl.gov/CMIP6/. The analysis codes, including Fortran program for solving the linearized omega equation and NCL script for computing the vorticity budget terms, are publicly available under an open-source license at Zenodo (https://zenodo.org/records/15123052).

Declarations

Competing interests
The authors declare no competing interests.

Received: 2 April 2025 Accepted: 14 May 2025
Published online: 29 May 2025

References

Adames ÁF, Wallace JM (2017) On the tropical atmospheric signature of El Niño. J Atmos Sci 74:1923–1939
Adler RF, Huffman GJ, Chang A, Ferraro R, Xie PP, Janowiak J, Rudolf B, Schneider U, Curtis S, Bolvin D, Gruber A, Susskind J, Arkin P, Nelkin E (2003) The version-2 global precipitation climatology project (GPCP) monthly precipitation analysis (1979-present). J Hydrometeorol 4:1147–1167
Chen W, Feng J, Wu R (2013) Roles of ENSO and PDO in the Link of the East Asian Winter Monsoon to the following Summer Monsoon. J Climate 26:622–635
Ding Y (1990) A statistical study of winter monsoons in East Asia. J Trop Meteor 6:119–128
Gao T, Zhang Q, Luo M (2020) Intensifying effects of El Niño events on winter precipitation extremes in southeastern China. Clim Dynam 54:631–648
Guo L, Zhu C, Liu B (2019) Possible causes of the flooding over south China during the 2015/2016 winter. Int J Climatol 39:3218–3230
Hersbach H, Bell B, Berrisford P, Hirahara S, Horányi A, Muñoz-Sabater J, Thépaut J-N et al (2020) The ERA5 global reanalysis. Q J Roy Meteor Soc 146:1999–2049
Hoskins B, Pedder M, Jones DW (2003) The omega equation and potential vorticity. Q J Roy Meteor Soc 129:3277–3303
Hu K, Huang G, Wu R, Wang L (2018) Structure and dynamics of a wave train along the wintertime Asian jet and its impact on East Asian climate. Clim Dynam 51:4123–4137
Huang RH, Chen W, Yang BL, Zhang RH (2004) Recent advances in studies of the interaction between the east Asian winter and summer monsoons and ENSO cycle. Adv Atmos Sci 21:407–424
Huang BC, Su T, Zhi R, Zhang ZP, Shen HY, Wu YP, Feng TC (2023) Synergistic effect of El Nino Southern oscillation and subtropical Indian Ocean Dipole on Southern China winter precipitation. Atmos Res 293:106928
Ke Z, Jiang X, Wang Z (2019) Southeastern China Boreal winter precipitation anomalies are dependent on intensity of El Niño. Sci Rep 9:17410
Kosaka Y, Nakamura H (2006) Structure and dynamics of the summertime Pacific-Japan teleconnection pattern. Q J Roy Meteor Soc 132:2009–2030
Kosaka Y, Nakamura H (2010) Mechanisms of meridional teleconnection observed between a summer monsoon system and a subtropical anticyclone. part I: the Pacific-Japan pattern. J Climate 23:5085–5108
Kuramochi M, Ueda H (2023) Two types of wintertime teleconnection patterns over the Western North Pacific associated with regionally different heating anomalies. J Meteorol Soc Jpn 101:21–37
Li C, Ma H (2012) Relationship between ENSO and winter rainfall over Southeast China and its decadal variability. Adv Atmos Sci 29:1129–1141
Li C, Sun JL (2015) Role of the subtropical westerly jet waveguide in a Southern China heavy rainstorm in december 2013. Adv Atmos Sci 32:601–612
Li T, Wang B, Wu B, Zhou TJ, Chang CP, Zhang RH (2017) Theories on formation of an anomalous anticyclone in Western North Pacific during El Nino: a review. J Meteorol Res 31:987–1006
Li X, Wen Z, Huang W-R (2020) Modulation of South Asian jet wave train on the extreme winter precipitation over Southeast China: comparison between 2015/16 and 2018/19. J Climate 33:4065–4081
Liu G, Ji L, Wu R (2012) An east-west SST anomaly pattern in the midlatitude North Atlantic Ocean associated with winter precipitation variability over eastern China. J Geophys Res Atmos 117(D15). https://doi.org/10.1029/2012JD017960
Liu Y, Hu Z-Z, Wu R (2020) Cooperative effects of tropical Pacific and Atlantic SST forcing in southern China winter precipitation variability. Clim Dynam 55:2903–2919. https://doi.org/10.1007/s00382-020-05430-z
Lu B, Scaife AA, Dunstone N, Smith D, Ren H-L, Liu Y, Eade R (2017) Skillful seasonal predictions of winter precipitation over southern China. Environ Res Lett 12:074021
Rayner NA, Parker DE, Horton EB, Folland CK, Alexander LV, Rowell DP, Kaplan A et al (2003) Global analyses of sea surface temperature, sea ice, and night marine air temperature since the late nineteenth century. J Gerontol Ser A Biol Med Sci 108:4407–4444
Sardeshmukh PD, Hoskins BJ (1988) The generation of global rotational flow by steady idealized tropical divergence. J Atmosp Sci 45:1228–1251
Sekizawa S, Nakamura H, Kosaka Y (2021) Remote influence of the interannual variability of the Australian Summer monsoon on wintertime climate in East Asia and the Western North Pacific. J Climate 34:9551–9570
Wang L, Chen W (2010) How well do existing indices measure the strength of the East Asian winter monsoon? Adv Atmos Sci 27:855–870
Wang L, Feng J (2011) Two Major Modes of the Wintertime Precipitation over China. Chin J Atmos Sci 35:1105–1116
Wang L, Lu M-M (2013) The East Asian Winter Monsoon. World Sci. https://doi.org/10.1142/9789813200913_0005
Wang B, Wu RG, Fu XH (2000) Pacific-East Asian teleconnection: how does ENSO affect East Asian climate? J Clim 13:1517–1536
Wu R, Hu ZZ, Kirtman BP (2003) Evolution of ENSO-related rainfall anomalies in East Asia. J Clim 16:3742–3758
Wu B, Li T, Zhou T (2010) Asymmetry of atmospheric circulation anomalies over the Western North Pacific between El Niño and La Niña*. J Clim 23:4807–4822
Wu B, Zhou TJ, Li T (2017) Atmospheric dynamic and thermodynamic processes driving the western north pacific anomalous anticyclone during El Nino. Part I: maintenance mechanisms. J Climate 30:9621–9635
Zhang R, Sumi A, Kimoto M (1996) Impact of El Niño on the East Asian monsoon : a diagnostic study of the '86/87 and '91/92 events. J Meteorol Soc Jpn 74:49–62
Zhang RH, Tian WS, He X, Qie K, Liu D, Tian HY (2021) Enhanced influence of ENSO on winter precipitation over Southern China in recent decades. J Clim 34:7983–7994
Zhou L (2010) Influence of South China Sea SST and ENSO on winter rainfall over South China. Adv Atmos Sci 27:832–844. https://doi.org/10.1007/s00376-009-9102-7
Zhou LT, Wu R (2010) Respective impacts of East Asian winter monsoon and ENSO on winter rainfall in China. J Geophys Res 115:D02107

Publisher's Note